SIMULATION OF WATER-ROCK INTERACTION IN THE YELLOWSTONE GEOTHERMAL SYSTEM USING TOUGHREACT

Patrick F. Dobson*, Sonia Salah, Nicolas Spycher, and Eric L. Sonnenthal

Earth Sciences Division, Lawrence Berkeley National Laboratory
1 Cyclotron Road
Berkeley, CA 94720, USA

ABSTRACT

The Yellowstone geothermal system provides an ideal opportunity to test the ability of reactive transport models to simulate the chemical and hydrological effects of water-rock interaction. Previous studies of the Yellowstone geothermal system have characterized water-rock interaction through analysis of rocks and fluids obtained from both surface and downhole samples. Fluid chemistry, rock mineralogy, permeability, porosity, and thermal data obtained from the Y-8 borehole in Upper Geyser Basin were used to constrain a series of reactive transport simulations of the Yellowstone geothermal system using TOUGHREACT. Three distinct stratigraphic units were encountered in the 153.4 m deep Y-8 drill core: volcaniclastic sandstone, perlitic rhyolitic lava, and nonwelded pumiceous tuff. The main alteration phases identified in the Y-8 core samples include clay minerals, zeolites, silica polymorphs, adularia, and calcite. Temperatures observed in the Y-8 borehole increase with depth from sub-boiling conditions at the surface to a maximum of 169.8°C at a depth of 104.1 m, with near-isothermal conditions persisting down to the well bottom. 1-D models of the Y-8 core hole were constructed to simulate the observed alteration mineral assemblage given the initial rock mineralogy and observed fluid chemistry and temperatures. Preliminary simulations involving the perlitic rhyolitic lava unit are consistent with the observed alteration of rhyolitic glass to form celadonite.

Keywords: water-rock interaction, Yellowstone, hydrothermal alteration, reactive transport modeling

INTRODUCTION

Yellowstone has been the site of extensive studies of hydrothermal alteration, including the examination of samples from 13 core holes drilled by the U.S. Geological Survey (White et al., 1975). The Y-8 core, consisting of three distinct geologic units (volcaniclastic sediments, perlitic rhyolitic lava, and nonwelded pumiceous ash-flow tuff), was selected for this modeling study. We chose to model water-rock interactions occurring within the perlitic rhyolitic lava. The lava was selected for the modeling study because both the primary (igneous) and secondary (alteration) minerals of this unit have been well characterized, and dissolution/precipitation processes occur under nearly isothermal conditions. The transition from a conductive to near-isothermal gradient near the upper boundary of the perlitic rhyolite suggests that convective fluid flow is restricted to the perlitic rhyolite lava and pumiceous tuff units (Dobson et al., 2003a). Detailed descriptions of the measured rock and water compositions and preliminary results of modeling conducted using the TOUGHREACT code are presented in the following sections.

* Corresponding author. Fax: (510) 486-5373, e-mail: pfdobson@lbl.gov

OBSERVED WATER-ROCK INTERACTION IN Y-8 CORE HOLE

The Y-8 core hole, located in the Upper Geyser Basin of the Yellowstone geothermal system, has been the subject of a variety of water-rock interaction studies. A general description of the stratigraphy is given by White et al. (1975), and consists of three main units: volcaniclastic sandstone (down to a depth of 55.2 m), perlitic rhyolitic lava (55.2–62.6 m), and pumiceous ash-flow tuff (62.6–153.4 m). White et al. (1975) also report the results of downhole temperature and pressure surveys. Temperatures increase with depth down to a depth of ~55 m, where near-isothermal conditions (160–170°C) persist down to the total depth of 153.4 m.

Detailed mineralogical descriptions of Y-8 core samples were presented by Keith et al. (1978) and Sturchio et al. (1986). Dobson et al. (2003a) characterized the permeability and porosity of Y-8 core samples and their relation to primary lithology and extent of hydrothermal alteration. Alteration has led to decreases in both permeability and porosity, and in some instances, to self-sealing resulting from the precipitation of silica.

Mineralogy of Y-8 Rhyolitic Lava

The perlitic rhyolitic lava and underlying pumiceous tuff encountered in the Y-8 core hole were correlated by Keith et al. (1978) with the 0.54 Ma Biscuit Basin rhyolite flow. Relatively unaltered samples of this flow were observed in the neighboring Y-7 drill core; the primary mineralogy of this unit is reported in Table 1. The alteration mineralogy of the rhyolitic lava observed in the Y-8 core consists of abundant celadonite (giving the cores a waxy, gray-green appearance), with lesser amounts of montmorillonite, silica polymorphs (quartz, cristobalite, chalcedony, and opal), zeolites (mordenite, clinoptilolite, and analcime), and adularia (Keith et al., 1978). Alteration is concentrated along hydration cracks in the perlitic glass and within veins and fractures (Figure 1). The rhyolitic lava was interpreted by Sturchio et al. (1986) to be cogenetic with the underlying pumiceous tuff, and thus the primary compositions of these two units is presumed to be similar. The rhyolitic lava and pumiceous tuff have similar alteration mineral assemblages, with the main difference being that the tuff has undergone more extensive alteration, resulting in the complete alteration of volcanic glass in this unit (Keith et al., 1978).

Porosity and Permeability of Y-8 Rhyolitic Lava

Dobson et al. (2003a) made a total of 6 porosity and 39 permeability measurements on perlitic rhyolitic core samples from the Y-8 well. Porosity measurements ranged from 3.4–16.2 %, with a mean value of 10.1 %. All but three of the permeability values were below 0.1 md (the detection limit of the minipermeameter used for most of the permeability measurements). The six values obtained for this unit using a conventional permeameter (with a minimum detection limit of 0.5 μd) ranged from 0.003–0.020 md.

Y-8 Water Compositions

The compositions of water samples collected using a downhole sampler from the Y-8 well were reported by Fournier (1981), Sturchio et al. (1986), and Sturchio et al. (1989). The reported sampling depths for these samples were 61-73 m (Sturchio et al., 1989), 64 m (Fournier, 1981), and 153 m (Sturchio et al., 1986), thus falling within the stratigraphic interval represented by the rhyolitic lava and pumicous tuff. There is little compositional variability in the compositions of these fluids apart from the reported silica compositions (258-390 ppm), with a higher silica concentration reported by Sturchio el al. (1986) for the deeper downhole sample. Composite values derived primarily from the Sturchio el al. (1989) Y-8 water composition are presented in

Table 2. For comparison and use in the modeling effort, a non-thermal groundwater composition from a rhyolitic terrain (Taupo volcanic zone) is also presented.

PRELIMINARY MODELING OF WATER-ROCK INTERACTION

The TOUGHREACT simulator (Xu and Pruess, 2001a, b; Xu et al., 2003) was used for the water-rock reaction simulations. TOUGHREACT incorporates reactive chemistry and transport into the TOUGH2 code (Pruess, 1991), using a sequential iteration approach for coupling chemical transport and reaction. The fluid velocities and phase saturations are used for solving chemical transport after solution of the flow equations. Chemical transport is solved on a component by component basis (by advection and diffusion), and the resulting concentrations are substituted into the chemical reaction model. Newton-Raphson iteration is used to solve the system of chemical reaction equations on a grid-block by grid-block basis. The equation-of-state module EOS3, which considers the fully coupled flow of water, air and heat, was used for all simulations. TOUGHREACT allows for the selection of either kinetic or equilibrium thermodynamics to be used for mineral dissolution and precipitation. In this preliminary work we did not consider changes in redox state, so all iron (both in mineral and dissolved species) is represented as ferric iron.

Thermodynamic and kinetic data from various literature sources (as tabulated in Spycher and Sonnenthal, 2003) were employed in the simulations. Four of the considered minerals (anhydrite, goethite, calcite, and hematite) were set to react at equilibrium with the aqueous phase. Other minerals (amorphous silica, α-cristobalite, microcline, albite, Ca-, Na-, and Mg-smectite, illite, quartz, rhyolitic glass, enstatite, diopside, plagioclase (Ab80An20), stellerite, heulandite, mordenite, analcime, clinoptilolite, kaolinite, fluorite, and celadonite) were set to react under kinetic constraints. The solubility constant of the glass was calculated using a modified version of the Techer et al. (2001) method (Salah et al., in prep.) and microprobe analyses of unaltered glass from the Biscuit Basin rhyolite (Sturchio et al., 1986).

Water-rock interactions were evaluated in two steps. First, the saturation states of minerals in the Y-8 geothermal fluid were computed at reservoir temperatures. This allowed us to determine which mineral phases would likely be dissolving (undersaturation) or precipitating (supersaturation). Next, a dilute groundwater composition was numerically reacted with the primary Y-8 mineralogy at 170°C. Using this methodology, the evolution of fluid and rock compositions with time could be evaluated and compared with the observed 'final' water and rock compositions of the Yellowstone geothermal system. Reactions with a gas phase were not considered for this preliminary work.

Determination of Mineral Saturations for Y-8 Geothermal Water

This simple model evaluated the degree of saturation in the reconstituted Y-8 water for each of the minerals considered in this study. First, the Y-8 water composition (Table 2) was speciated using a temperature of 170°C. Then, the model was run for 1 second to preclude water-rock interaction, and log (Q/K) values of the initial minerals present in the rock as well as potential secondary phases were examined (Table 3). Rhyolitic glass and potassium feldspar are undersaturated, and thus are predicted to dissolve, while the secondary minerals calcite, albite, and celadonite are oversaturated, and predicted to precipitate from this water. The geothermal water is near equilibrium with respect to the minerals plagioclase (Ab80An20), quartz, illite, and fluorite. None of the zeolitic phases evaluated were supersaturated in the thermal water.

Simulation of Water-Rock Interaction Using 1-D Plug Flow Model

A plug-flow model similar to that used by Dobson et al. (2003b) was employed to evaluate chemical changes in both water and rock composition resulting from water-rock interaction. For this simplified model, an isothermal (170°C) 1-D plug flow model was constructed with 5 rock elements. Dilute groundwater (Table 2) was injected in the first element at a constant rate, with a correspondingly slow seepage velocity (~3.5×10^{-8} m/s) to facilitate water-rock interaction. The last rock element was assigned a large volume (>10^{50} m^3) to act as a constant pressure boundary. The simulation was run for 579 years. Although this is a relatively short time period on the time scale of most geothermal systems (thousands to hundreds of thousands of years), it is sufficient to permit water-rock interaction. Changes in fluid compositions and mineral abundances were monitored in the first and fourth rock blocks throughout the simulation.

Simulated changes in mineralogy

The dominant process observed in the simulation was the dissolution of rhyolitic glass, the primary mineral constituent of the rock, with over 95% of the glass dissolved after 50,000 days (Figure 2). Because the plug flow simulation used a matrix flow model with correspondingly elevated mineral surface areas, the rate of glass dissolution is greatly enhanced. Other primary mineral phases undergoing dissolution include quartz, enstatite, plagioclase, hematite, microcline, and diopside (except in the first rock element).

The simulation also resulted in the precipitation of several secondary mineral phases. Illite and celadonite, the most abundant alteration phase in the Y-8 rhyolitic lavas, were the two main aluminosilicate minerals formed. Goethite, used as a proxy for iron-bearing secondary mineral phases, also precipitated during the simulation. None of the zeolites observed in the core samples (mordenite, clinoptilolite, and analcime) was produced in the simulation.

Simulated changes in fluid chemistry

Changes in fluid chemistry in the plug-flow simulation were monitored over time in the fourth element block, where the most pronounced changes in fluid chemistry were expected. Most dissolved species experience rapid initial changes in concentration, followed by the development of nearly steady-state conditions. The evolved water composition at the end of the simulation (Table 4) is very similar in many components to the initial dilute fluid (Table 2), reflecting the elevated integrated water-rock ratio for this simulation. Although some species experience increases in concentration resulting from mineral dissolution, other species, such as chloride and sodium, never approach the elevated concentrations observed in the Y-8 geothermal water.

Sensitivity to changes in thermodynamic parameters

As a sensitivity test to changes in the thermodynamic characterization of mineral phases, the simulation used to evaluate the degree of mineral saturation of the Y-8 water was repeated using thermodynamic data for calcium clinoptilolite in lieu of the clinoptilolite phase used in the initial simulations (Table 3). There are slight differences in chemistry between these two phases: the calcium clinoptilolite has minor amounts of iron and no potassium and sodium, while the clinoptilolite composition used in the initial runs has minor amounts of potassium and sodium, but is iron-free. The calcium clinoptilolite data were obtained from the EQ3/6 database data0.ymp.R2, as derived from Viani and Bruton (1992). The results of this run, as indicated by Simulation 2 in Table 3, indicate that clinoptilolite is stable and expected to precipitate. This

result demonstrates the degree of sensitivity that simulations of water-rock interaction have to the thermodynamic data used to represent mineral phases and dissolved species.

DISCUSSION AND CONCLUSIONS

This work represents a preliminary attempt to model water-rock interaction at Yellowstone. These simulations capture the dominant mineral phases undergoing dissolution and precipitation in the rhyolitic lava. However, precipitation of the zeolites clinoptilolite, mordenite, and analcime, which were observed in the Y-8 core samples, was not predicted for the initial simulations. Substitution of different thermodynamic data and composition for clinoptilolite resulted in its precipitation, thus emphasizing the sensitivity of reactive transport models to these data.

There are a number of possible explanations for the discrepancies between the simulated and observed water-rock interaction. The sampled Y-8 water composition was assumed to have reacted with the rhyolitic lava unit. As noted earlier, there are three distinct rock units present in the Y-8 core hole, and minerals found in the other two units may control the fluid composition, although the lower pumiceous unit is quite similar in composition. Although a downhole sampler was used to collect the water samples, boiling may have altered the water sample compositions.

A number of simplifications were made in the water-rock simulations. Stoichiometric end-member compositions were used for most of the minerals, but many of the actual observed primary and secondary mineral phases have intermediate compositions. Gas species were not included in these simulated reactions. Ion exchange reactions were also not considered in these simulations. Assumed reactive surface areas were used to simulate kinetic mineral reactions. Development of a more rigorous precipitation rate law that includes surface free energy effects as a function of particle size and surface area may improve predictions of clay and zeolite precipitation. The use of a modified plug flow model that incorporates the low permeability and porosity characteristics of the perlitic rhyolitic lava would result in more realistic reaction rates for glass dissolution. The higher permeability, porosity, reactive surface area, and extent of hydrothermal alteration observed for the underlying pumiceous tuff suggests that this compositionally similar unit may have a stronger influence on the water composition than the perlitic rhyolite lava.

Future modeling of water-rock interaction at Yellowstone can address some of the simplifications mentioned above. The ultimate goal of this work is to capture the relation between hydrothermal alteration and changes in permeability and porosity observed in the Yellowstone geothermal system.

ACKNOWLEDGMENTS

We thank Terry Keith and Tom Michalski of the USGS for facilitating the initial study of the Y-8 core. Tim Kneafsey and Jeff Hulen participated in the characterization of the Y-8 core samples. John Apps was the primary developer of the mineral thermodynamic database employed in this study. Stefan Finsterle and Kevin Knauss provided helpful comments through their reviews of this manuscript, and Diana Swantek provided assistance with the illustrations. This work was supported by the Director, Office of Civilian Radioactive Waste Management, U.S. Department of Energy, through Memorandum Purchase Order EA9013MC5X between Bechtel SAIC Company, LLC, and the Ernest Orlando Lawrence Berkeley National Laboratory

(Berkeley Lab). The support is provided to Berkeley Lab through the U.S. Department of Energy Contract DE-AC03–76SF00098.

REFERENCES

Dobson, P.F., Kneafsey, T.J., Hulen, J., Simmons, A., 2003a. Porosity, permeability, and fluid flow in the Yellowstone geothermal system, Wyoming. Journal of Volcanology and Geothermal Research 123, 313–324.

Dobson, P.F., Kneafsey, T.J., Sonnenthal, E.L., Spycher, N., Apps, J.A., 2003b. Experimental and numerical simulation of dissolution and precipitation: implications for fracture sealing at Yucca Mountain, Nevada. Journal of Contaminant Hydrology 62–63, 459–476.

Fournier, R.O., 1981. Application of water geochemistry to geothermal exploration and reservoir engineering. In: Rybach, L., Muffler, L.J.P (Eds.), Geothermal Systems: Principles and Case Histories. John Wiley and Sons, pp. 109–143.

Keith, T.E.C, White, D.E., Beeson, M.H., 1978. Hydrothermal alteration and self-sealing in Y-7 and Y-8 drill holes in northern part of Upper Geyser Basin, Yellowstone National Park, Wyoming. U.S. Geological Survey Professional Paper 1054-A, 26 pp.

Pruess, K., 1991. TOUGH2—a general-purpose numerical simulator for multiphase fluid and heat flow. Rep. LBL-29400, Lawrence Berkeley National Laboratory, Berkeley, CA, 1991.

Salah, S., Spycher, N., Sonnenthal, E., Apps, J., in prep. Glass/tuff alteration mechanisms and plug-flow reactor simulations.

Spycher, N., Sonnenthal, E., 2003. Drift-scale coupled processes (DST and THC seepage) models. MDL-NBS-HS-000001 REV02 ICN00. Bechtel SAIC Company (BSC), Las Vegas, NV.

Sturchio, N.C., Muehlenbachs, K., Seitz, M.G., 1986. Element redistribution during hydrothermal alteration of rhyolite in an active geothermal system: Yellowstone drill cores Y-7 and Y-8. Geochimica et Cosmochimica Acta 50, 1619–1631.

Sturchio, N.C., Bohlke, J.K., Binz, C.M., 1989. Radium-thorium disequilibrium and zeolite-water ion exchange in a Yellowstone hydrothermal environment. Geochimica et Cosmochimica Acta 53, 1025–1034.

Techer, I., Advocat, T., Lancelot, J., Liotard, J.-M., 2001. Dissolution kinetics of basaltic glasses: control by solution chemistry and protective effect of the alteration film. Chemical Geology 176 (1–4), 235–263.

Timperley, M.H., 1983. Phosporous in spring waters of the Taupo Volcanic Zone, North Island, New Zealand. Chemical Geology 38, 287–306.

Viani, B.E. and Bruton, C.J. 1992. Modeling Fluid-Rock Interaction at Yucca Mountain, Nevada: A Progress Report. UCRL-ID-109921. Livermore, California: Lawrence Livermore National Laboratory.

White, D.E., Fournier, R.O., Muffler, L.J.P., Truesdell, A.H., 1975. Physical results of research drilling in thermal areas of Yellowstone National Park, Wyoming. U.S. Geological Survey Professional Paper 892, 70 pp.

Xu, T., Pruess, K., 2001a. Modeling multiphase non-isothermal fluid flow and reactive geochemical transport in variably fractured rocks: 1. Methodology. American Journal of Science 301, 16–33.

Xu, T., Pruess, K., 2001b. On fluid flow and mineral alteration in fractured caprock of magmatic hydrothermal systems. Journal of Geophysical Research 106 (B2), 2121–2138.

Xu, T., Sonnenthal, E., Spycher, N., and Pruess, K., 2003. TOUGHREACT: A new code of the TOUGH family of non-isothermal multiphase reactive geochemical transport in variably saturated geologic media. Proceedings, TOUGH Symposium 2003, Lawrence Berkeley National Laboratory, Berkeley, California, May 12–14, 2003.

Figure Captions

Figure 1. Photomicrograph of perlitic rhyolitic lava from Y-8 core at 61.37 m depth. Euhedral plagioclase crystals are in a glassy groundmass. Celadonite alteration is concentrated along perlitic cracks. Bottom length is 3.2 mm.

Figure 2. Simulated changes in abundance of primary and secondary minerals in the fourth plug-flow rock element. Smectite, stellerite, kaolinite, and microcline exhibit minimal change in abundance. Minerals with no measured change in abundance are not plotted.

Table Captions

Table 1. Mineralogy and Corresponding Thermodynamic Representation for Y-8 Rhyolite Lava.

Table 2. Initial Water Compositions.

Table 3. Mineral Saturations in Y-8 Water.

Table 4. Simulated Water Compositions.

Figures

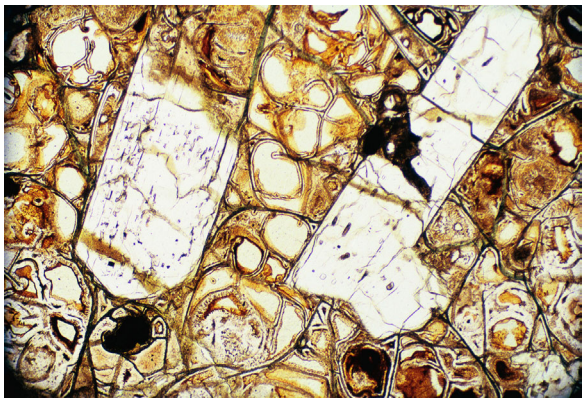

Figure 1.

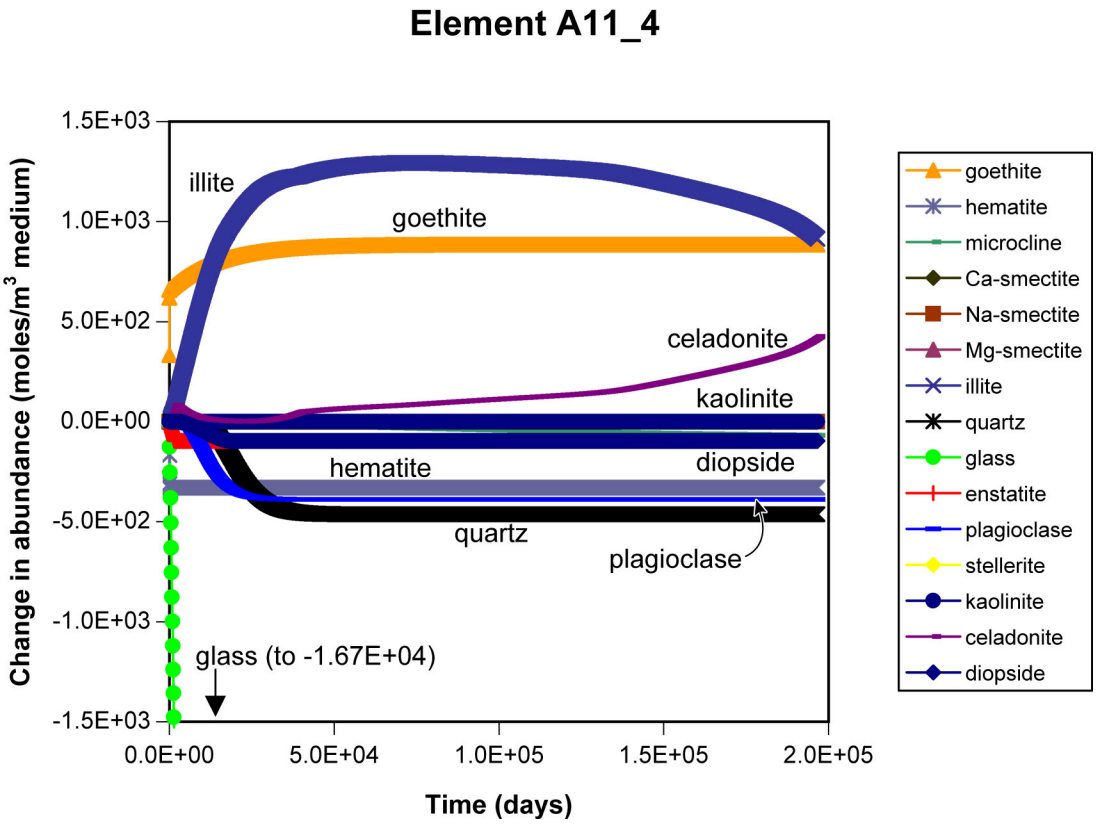

Figure 2.

Tables

Table 1

Mineral	Model Mineral	Abundance (vol. %)
Rhyolitic glass	Rhyolitic glass	82.3
Plagioclase	Ab80An20	7.8
Sanidine	Microcline	2.3
Quartz	Quartz	2.1
Clinopyroxene	Diopside	2.8
Fe-Ti oxides	Hematite	2.0
Orthopyroxene	Enstatite	0.6

Primary mineralogy of Y-8 perlitic rhyolitic lava from Sturchio et al. (1986).

Table 2

Species (molal)	Y-8 water	Groundwater
Cl^-	6.685e-03	7.33e-05
F^-	1.474e-03	1.74e-05
HCO_3^-	8.407e-03	6.49e-04
SO_4^{-2}	1.561e-04	3.23e-05
SiO_2 (aq.)	4.827e-03	1.05e-03
AlO_2^-	5.559e-06	1.11e-07
Ca^{+2}	8.483e-05	7.24e-05
Mg^{+2}	9.052e-06	5.35e-05
$HFeO_2$ (aq.)	5.372e-06	1.79e-07
K^+	4.220e-04	3.58e-05
Na^+	1.618e-02	4.57e-04
pH	7.26	7

Data for Y-8 water from Fournier (1981), Sturchio et al. (1986), and Sturchio et al. (1989). Data for cold groundwater from Timperley (1983).

Table 3

	Simulation 1		Simulation 2	
Mineral Phase	+ Log (Q/K)	- Log (Q/K)	+ Log (Q/K)	- Log (Q/K)
Rhyolitic glass		-2.808		-2.808
Ab80An20	0.047		0.047	
Microcline		-0.983		-0.983
Quartz	0.193		0.193	
Diopside	2.581		2.581	
Hematite	6.186		6.186	
Enstatite	0.838		0.838	
Anhydrite		-2.273		-2.273
Goethite	2.439		2.439	
Calcite	0.774		0.774	
Amor. silica		-0.426		-0.426
α-cristobalite		-0.140		-0.140
Albite	0.345		0.345	
Ca-smectite		-1.065		-1.065
Na-smectite		-1.324		-1.324
Mg-smectite		-1.004		-1.004
Illite		-0.088		-0.088
Stellerite		-0.225		-0.225
Heulandite		-1.287		-1.287
Mordenite		-1.691		-1.691
Analcime		-5.707		-5.707
Clinoptilolite[1]		-1.564	5.449	
Kaolinite		-1.158		-1.158
Fluorite		-0.094		-0.094
Celadonite	2.320		2.320	

Primary phases are highlighted in bold.

[1] Simulation 1 used thermodynamic data for iron-free Ca-clinoptilolite with minor amounts of Na and K; Simulation 2 used data for iron-bearing Ca-clinoptilolite. See text for discussion.

Table 4

Species (molal)	Range of simulated values	Value at end of simulation
Cl^-	7.33e-5 – 7.43e-5	7.33e-5
F^-	1.74e-5 – 1.76e-5	1.74e-5
HCO_3^-	5.57e-4 – 7.13e-4	6.49e-4
SO_4^{-2}	3.23e-5 – 3.27e-5	3.23e-5
SiO_2 (aq.)	1.05e-3 – 4.66e-3	1.11e-3
AlO_2^-	1.11e-7 – 1.39e-4	4.98e-5
Ca^{+2}	5.93e-5 – 1.39e-4	7.24e-5
Mg^{+2}	4.97e-11 – 5.46e-5	4.43e-5
$HFeO_2$ (aq.)	9.05e-9 – 1.79e-7	9.16e-9
K^+	9.41e-6 – 2.37e-4	3.66e-5
Na^+	4.57e-4 – 9.18e-4	4.57e-4
pH	7.00 – 7.61	7.07